ChemCatChem

Research Article
doi.org/10.1002/cctc.202400251

Chemistry Europe
European Chemical Societies Publishing

www.chemcatchem.org

Sulfonated Graphene-Based Materials as Heterogeneous Acid Catalysts for Solketal Synthesis by Acetalization of Glycerol

Dolores G. Gil-Gavilán,[a] Juan Amaro-Gahete,*[a, b] Raúl Rojas-Luna,[a] Almudena Benítez,[c] Rafael Estevez,*[a] Dolores Esquivel,[a] Felipa M. Bautista,[a] and Francisco J. Romero-Salguero*[a]

Acid catalysis plays a pivotal role in the industrial landscape due to its multifaceted contributions to various chemical processes in numerous sectors, including petrochemicals, polymers, food processing, and biodiesel production, among others. Sulfonated graphenes hold notable relevance as heterogeneous acid catalysts due to their unique combination of graphene's structural properties and the introduction of sulfonic groups as catalytic acid sites. Herein, we report the preparation of three sulfonated graphene-based materials – sulfonated reduced graphene oxide (rGO-SO_3H), chlorosulfonated reduced graphene oxide (rGO-HSO_3Cl) and sulfonated graphene oxide (GO-SO_3H) – by different synthetic approaches. Physicochemical, textural, morphological, and acidic properties of all materials were characterized in detail by different instrumental techniques. Innovatively, these materials have been evaluated as heterogeneous acid catalysts in the solketal synthesis by acetalization of glycerol, which is considered an interesting building block to produce added-value products. The density of acidic active sites and hydrophobicity were found to be conditioning parameters of the resulting catalytic activity in terms of conversion and selectivity. The best catalytic performance was obtained by rGO-SO_3H, reaching the maximum conversion towards solketal in 15 minutes under mild reaction conditions. The reusability and stability of all materials were also examined after three consecutive acetalization reactions with only a slight loss of catalytic activity.

1. Introduction

Catalysis is a fundamental and indispensable field that profoundly impacts the world across numerous sectors, playing a significant role in reducing pollution of the environment and satisfying the current enormous energy demand.[1,2] Specifically, acid catalysis holds great significance in several industrial processes ranging from oil refining and pharmaceutical manufacturing to polymer production and food processing,[3] due to its ability to enhance reaction rates, control selectivity, and enable milder operating conditions. In this context, significant reaction types include Friedel–Crafts alkylations, acylations, and sulfonations, as well as aromatic halogenations, nitrations, isomerizations, and oligomerizations. Traditional mineral acids such as sulfuric (H_2SO_4), phosphoric (H_3PO_4), hydrochloric (HCl) and hydrofluoric (HF) acids have been widely reported to catalyze these organic transformations with high efficiency at low economic cost.[4] However, the drawbacks of the homogeneous catalysis are currently well-known, including the difficulties in separating the catalysts from the resulting products, the need to carry out additional neutralization steps to prevent the corrosion of the equipments and the production of large volume of toxic and corrosive wastes.[5,6]

Since 1940, there has been an increasing tendency to replace these mineral acids by solid acids whenever feasible, which present clear advantages from an environmental point of view.[7] Heterogeneous catalysis promoted by acid solids finds broad applications in numerous acid-promoted processes within organic synthesis and has emerged as crucial materials due to its many advantages, including: i) straightforward product separation from the reaction medium; ii) the ability to easily recover and reuse the catalyst multiple times without any loss

[a] D. G. Gil-Gavilán, Dr. J. Amaro-Gahete, R. Rojas-Luna, Prof. R. Estevez, Prof. D. Esquivel, Prof. F. M. Bautista, Prof. F. J. Romero-Salguero
Departamento de Química Orgánica, Instituto Químico para la Energía y el Medioambiente (IQUEMA)
Facultad de Ciencias, Universidad de Córdoba, Campus de Rabanales, Edificio Marie Curie, E-14071 Córdoba, Spain
E-mail: q22amgaj@uco.es
q72estor@uco.es
qo2rosaf@uco.es

[b] Dr. J. Amaro-Gahete
UGR-Carbon – Materiales Polifuncionales Basados en Carbono, Departamento de Química Inorgánica
Unidad de Excelencia Química Aplicada a Biomedicina y Medioambiente, Universidad de Granada, ES18071, Granada, Spain

[c] Dr. A. Benítez
Departamento de Química Inorgánica e Ingeniería Química, Instituto Químico para la Energía y el Medioambiente (IQUEMA)
Facultad de Ciencias, Universidad de Córdoba, Campus de Rabanales, Edificio Marie Curie, E-14071 Córdoba, Spain

Supporting information for this article is available on the WWW under https://doi.org/10.1002/cctc.202400251

of activity; iii) the propensity for clean reactions resulting in high-purity products; iv) the reduction of corrosion problems in the reactor and the plant; and v) the capability to promote selective reactions.[5,8–10] The Brønsted/Lewis acidity, the population and strength of active sites, and the structure of the support material related to its surface area and porosity are tunable properties to obtain the highest product selectivity.

Regarding the solid acids, and the accessibility and effective dispersion of active sites, a wide variety of inorganic materials with different surface areas and average pore diameters, including zeolites,[11,12] silicas,[13,14] cation-exchange resins,[15] polymers,[16] hydroxyapatite,[17] zirconia,[18] heteropolyacids,[19] sulfated metal oxides,[18] organic-inorganic composites,[20] and carbons,[21] have been successfully employed as catalytic supports.

Focusing on carbon-based supports for acid catalysis, it is worth mentioning that prior to the 21st century, the carbon family was predominantly characterized by well-known materials such as graphite, diamond, fullerenes, and carbon nanotubes. However, this perception underwent a transformation with the groundbreaking isolation of free-standing 2D graphene in 2004 by Andre Geim, Konstantin Novoselov and co-workers.[22] Graphene is a two-dimensional allotrope of carbon, consisting of a single layer of carbon atoms arranged in a hexagonal lattice and is often described as a "wonder material" due to its exceptional properties, such as high strength, lightweight, high electrical and thermal conductivity, transparency, flexibility, impermeability, large surface area, chemical stability and biocompatibility.[23,24] However, there are many limitations to produce high-purity graphene by traditional bottom-up approaches (confined self-assembly, chemical vapor deposition (CVD), arc discharge, epitaxial growth on silicon carbide (SiC), etc.) because of production costs, restricted scalability, poor layer uniformity, lack of standardization for characterizing and defining graphene quality, contamination from residual chemicals, metals, or other carbon structures, and the presence of structural defects.[25] To overcome these drawbacks, graphene oxide (GO) and reduced graphene oxide (rGO) have emerged in recent decades as promising graphene-derived materials with high functionalization capacity, dispersibility, versatility, processability, and tailored electrical conductivity properties, which are produced at large-scale and high cost-effectiveness.[26,27] Whilst GO has oxygen-containing functional groups, such as hydroxyl (–OH), epoxide (–O–), and carboxyl (–COOH) groups, attached to the carbon lattice that introduce defects and disrupt the perfect hexagonal structure of graphene, rGO is obtained by reducing graphene oxide, which removes some of the oxygen functional groups, partially restoring the sp^2 carbon-carbon bonds found in pristine graphene.[28–30] Therefore, the notion of carbocatalysis within the framework of graphene-based material represents a burgeoning research field that is relatively new but rapidly gaining prominence in organic chemistry, materials science and green chemistry. Thus, graphene-based acid catalysis has garnered significant interest in the field of heterogeneous catalysis due to its unique electronic and surface properties noted above, wide commercial availability and environmental acceptability.[31–33]

Since the pioneering applications by Hara and co-workers as solid Brønsted acid catalysts in 2004,[34] the area of heterogeneous carbocatalysis using SO_3H-containing acidic carbons has expeditiously progressed for many important organic reactions (esterification, transesterification, etherification, acetalization) replacing the rare earth and noble metals frequently employed as catalysts in industrial operations. To sulfonate carbon supports, sulfonating agents such as concentrated H_2SO_4, fuming H_2SO_4, gaseous sulphuric anhydride (SO_3), chlorosulfonic acid (HSO_3Cl), p-toluenesulfonic acid, or aryl diazonium salts containing SO_3H, among others, are commonly employed. Templated carbons such as ordered mesoporous carbons and zeolite-templated carbons, commercial carbon supports such as glassy carbons, activated carbons, carbon foams, and carbon fibers, as well as nanostructured carbons such as graphene, graphene oxide, nanotubes, and carbon dots have been used as sulfonated platforms to prepare carbon-based acid catalysts.[21]

In this scenario, sulfonated graphene-based materials represent an emerging category of metal-free solid protonic acids characterized by their distinctive carbon structure and strong Brønsted acidity with Hammett strength ($-H_0$) = 8–11 comparable to concentrated H_2SO_4.[35] These supports with graphene nature, featuring covalently attached SO_3H groups through C–$PhSO_3H$ or C–SO_3H bonds, exhibit remarkable versatility as solid acids that can withstand water exposure.[36] Specifically, GO and rGO are currently considered attractive platforms to tether catalytically active species due to their low-cost and large-scale production, unique surface chemistry, high chemical and thermal stability, and tailorable pore structures, positioning them as promising alternatives to liquid H_2SO_4 in many industries involving catalytic reactions.[21] In fact, the catalytic activity of sulfonated graphene oxide surpasses that of other solid acid catalysts and traditional sulfuric acid, which can be attributed to the creation of hydrophobic cavities on the sulfonated graphene oxide surface, resulting from the combination of graphene nanosheets and oxygen-containing groups. These cavities facilitate the catalyst interaction with substrates/reactants and significantly enhance proton interactions, promoting high catalytic reactivity.[37] Commonly, the sulfonation procedure for these materials can be carried out by two different routes: (i) the direct sulfonation of GO, and (ii) the reduction of GO to rGO and subsequent sulfonation of rGO.[38]

Herein, several sulfonated graphene-based materials have been tested in the acetalization of glycerol with acetone, which yields mainly the five-member ring (1,3-dioxolane or solketal) as major product, and the six-member ring in a lower amount (1,3-dioxane). Solketal has attracted significant attention since it can be used as a smart building block to produce added-value products and fine chemicals.[39–41] Among the different uses, solketal has been tested as an oxygenated additive for (bio)fuels,[42,43] since it is able to diminish the particulate matter emission and also improve the flow properties and the oxidation stability of fuels.[44] Furthermore, because of its low toxicity, solketal is employed as an environmentally friendly

solvent in various industrial processes, including those in pharmaceuticals, polymers, cleaning products, and pesticides. Finally, recycling experiments were performed to evaluate the stability of the sulfonated graphene-based materials under reaction conditions.

2. Results and Discussion

2.1. Characterization

Different sulfonated graphene-based materials have been synthesized according to the detailed procedure described in experimental section (Figure 1). Firstly, GO was prepared by modified Hummers method in which graphite was exfoliated and functionalized with oxygenated groups. The hydrothermal treatment at 200 °C and subsequent reaction with fuming H_2SO_4 gave place to the sulfonated reduced graphene oxide (rGO-SO_3H). On the other hand, a direct sulfonation of GO was carried out by reaction with chlorosulfonic acid (HSO_3Cl) obtaining chlorosulfonated reduced graphene oxide (rGO-SO_3H). Alternatively, GO was subjected to a thiolation process using hydrobromic acid and thiourea as reagents. The subsequent oxidation step of this material with hydrogen peroxide (H_2O_2) resulted in the sulfonated graphene oxide (GO-SO_3H).

XRD analyses were carried out to study the crystal structure of the synthesized materials (Figure 2 and Figure S1). The successful insertion of the oxygenated groups between graphitic sheets leading to the separation and disordering of the crystalline laminar structure[45,46] was confirmed due to the disappearance of the peak at 26.4° ($d = 0.34$ nm), associated to the pristine graphitic structure[47] (Figure S1). Thus, the GO pattern displayed a new prominent peak at 11.7°, related to the 001 plane, which corresponds with an interlayer distance of $d = 0.76$ nm.[48] This new signal is indicative of a well-stacked layered structure with different oxygenated groups such as hydroxyl, epoxy, carboxyl and carbonyl. The reduction of oxygenated groups involved the replacement of the 11.7° diffraction peak in the rGO diffraction pattern, associated with GO, for a broad band centered at 25.3° ($d = 0.35$ nm),[49] which was attributed to 002 plane,[50] thereby confirming further interlayer separation, effective thermal exfoliation of GO and elimination of most of the oxygenated groups.[46,51] This broad peak revealed small 2D crystallites, which is indicative of lattice strain and defects.[49] The absence of the peak at 11.7° in rGO suggested a significant alteration with respect to GO through the acquisition of hydrophobic properties.[52] The thiolation of GO can be directly achieved by transforming hydroxyl functional groups.[53] After the thiolation and the subsequent reduction process suffered by GO, the resulting rGO-SH material exhibited two signals at 24.1° and 42.9°,[54] analogously to the reduced graphene oxide.

The XRD pattern of the rGO-SO_3H displayed two bands at 25.3° ($d = 0.35$ nm) and 43.4° associated with 002 and 100

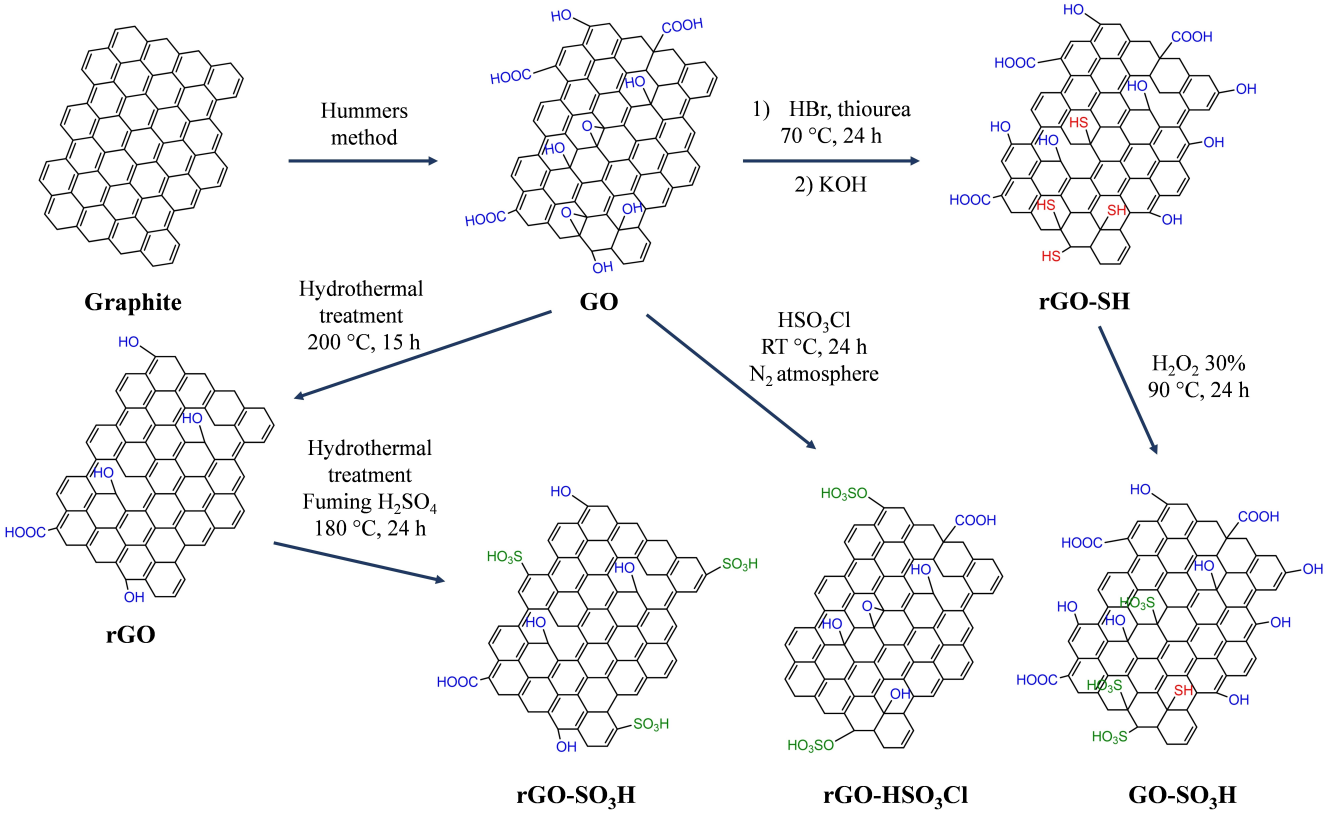

Figure 1. Synthetic routes used to obtain sulfonated graphene materials.

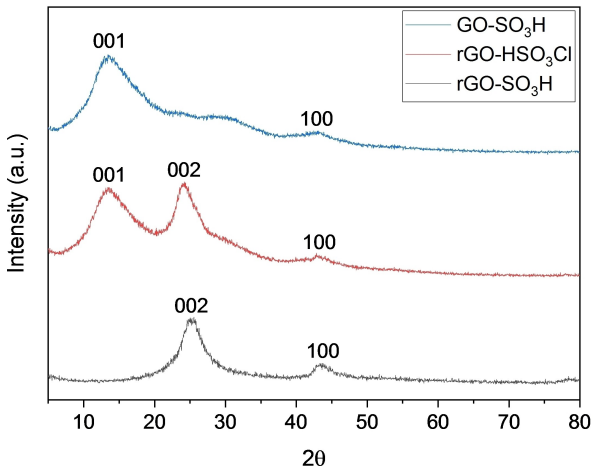

Figure 2. XRD patterns of the sulfonated graphene materials.

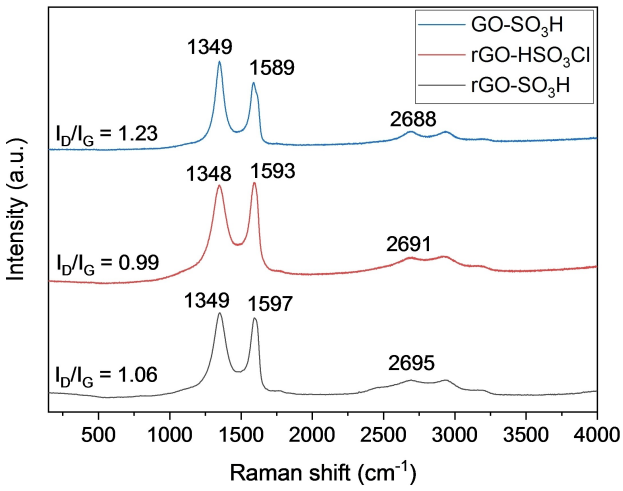

Figure 3. Raman spectra of the sulfonated graphene materials.

planes typical of reduced graphene oxide (Figure 2).[55] These two signals were also showed by rGO-HSO_3Cl in addition to a band at 13.6° (d = 0.65 nm) associated to 001 plane characteristic of graphene oxide,[56] thus confirming that graphene oxide in this material was partially reduced during the substitution of oxygenated groups with $-OSO_3H$ groups.[57] The GO-SO_3H diffraction pattern exhibited two bands at 13.5° (d = 0.66 nm) and 43.4° typical of 001 and 100 planes, respectively, which is in accordance with an oxidized graphene XRD pattern.[58] This is because the thiol-functionalized rGO (rGO-SH) was reoxidized by the H_2O_2 treatment.[59] XRD patterns revealed a decrease in the crystallinity degree of the material when functionalized with oxygen and sulfur atoms.[60]

Raman spectra of the synthesized materials are shown in Figure 3 and Figure S2. Graphene-based materials exhibited D and G bands as the main signals at 1349 cm^{-1} and 1590 cm^{-1}, respectively, which are assigned to sp^3 and sp^2 carbon domains (Figure S2).[61] D band is associated with defects and disorder while G band is related to the 2D graphitic hexagonal lattice. Moreover, these materials presented a band around 2680 cm^{-1}, denoted 2D band, which is an overtone of D band.[45] Raman spectra of rGO-SH provided additional confirmation of the correct thiol functionalization due to the appearance of new peaks, specifically at 621 and 975 cm^{-1}, which evidenced the formation of C–S bonds.[47] Intensities ratio of D and G bands (I_D/I_G) gives information about the disorder of graphene-based compounds,[36] with higher I_D/I_G ratio for a more disordered material. Graphite presented a I_D/I_G ratio of 0.28 whereas the values for GO, rGO and rGO-SH were 0.86, 1.01 and 1.11, respectively (Figure S2).[46] The higher I_D/I_G ratio of rGO compared to that of GO is attributed to the decrease in the sp^2 graphitic domains and the increase in the crystal structure disorder during the reduction process.[62,63] In the sulfonated materials these values were 1.06, 0.99 and 1.23 for rGO-SO_3H, rGO-HSO_3Cl and GO-SO_3H, respectively (Figure 3). It is noteworthy that the functionalization with sulfur groups promoted the formation of sp^3 carbons after thiolation and sulfonation processes,[64,65] which resulted in higher I_D/I_G ratios compared to GO (0.86). The conservation of D and G bands corroborated that graphene structure remained unchanged after sulfonation process.[55]

The quantification of the sulfur species after the sulfonation processes was studied by elemental analysis, revealing a sulfur content of 2.07%, 1.09% and 3.62% in rGO-SO_3H, rGO-HSO_3Cl and GO-SO_3H, respectively, which confirmed that the sulfonation process was successful.[66]

Textural properties of the obtained materials were studied by nitrogen adsorption-desorption isotherms (Figure 4). Specific surface area and pore volume values are listed in Table 1. GO-SO_3H exhibited a combination of type II and IV isotherms with macropores and a wide mesopore distribution whereas rGO-SO_3H and rGO-HSO_3Cl only presented type IV isotherms, being rGO-SO_3H the material with the lowest pore size (most below 25 nm) (Figure 4).[67,68] GO-SO_3H exhibited a hysteresis loop of type H3 associated to non-rigid aggregates of plate-like particles, whereas rGO-HSO_3Cl and rGO-SO_3H gave H2 loops, which corresponded to non-homogeneous pore sizes and distributions.[69] The reduction of the oxygenated groups from

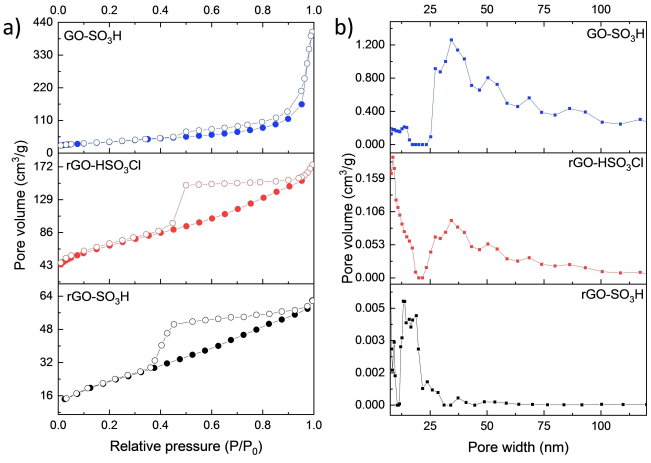

Figure 4. a) Nitrogen adsorption-desorption isotherms and b) pore size distributions obtained by a DFT method of the sulfonated graphene materials.

Table 1. Textural properties of the synthesized materials.

Sample	S_{BET} (m^2/g)	Pore volume (cm^3/g)
Graphite	19	0.06
GO	146	0.10
rGO	273	0.51
rGO-SO_3H	86	0.05
rGO-HSO_3Cl	245	0.27
rGO-SH	81	0.46
GO-SO_3H	134	0.63

GO to rGO led to an increase in surface area, while the functionalization step with fuming H_2SO_4 for obtaining rGO-SO_3H led to a slight decrease in surface area and pore volume with respect to the rGO material.[54] Probably, the heat treatment at 180 °C under strong acidic conditions could have contracted the pore volume of the material while the sulfonic groups could have anchored mainly on the surface, thus decreasing the available surface area. Unlike, the sulfonation treatment of GO under milder conditions with HSO_3Cl resulted in the sulfonated materials with the highest specific surface area (245 m^2/g). An increase of surface area was observed for GO-SO_3H after the oxidation step carried out in rGO-SH preserving most of the surface area of the starting GO with an increase in pore volume. The presence of macropores could explain the higher pore volume in GO-SO_3H.

Surface composition was analyzed by XPS to determine the oxidation states of the species after oxidation, thiolation and sulfonation processes (Figure S3). C 1s region of pristine graphite, GO and rGO materials could be fitted into five contributions associated with C=C/C–C (284.8 eV), C–O (286.6 eV), C=O (287.8 eV), COOH (288.9 eV), and π–π* (290.2 eV), respectively (Figure S4). The incorporation of thiol functional groups on rGO-SH gave rise to an additional contribution at 285.5 eV, characteristic of C–S bond. All these contributions were clearly present for sulfonated graphene-based materials (Figure 5).[70,71] A significant contribution of C–O was observed in GO C 1s spectra typical of hydroxyl and epoxy groups (Figure S4).[54,63] The bromination of GO determined the functionalization degree for both rGO-SH and GO-SO_3H due to the epoxy ring-opening and nucleophilic substitution of hydroxyl groups.[72] Interestingly, the presence of C–O contribution in rGO-SH confirmed the difficulty of a total replacement of the hydroxyl groups by thiol groups.[73] The appearance of sulfur contributions indicated that the thiolation and sulfonation processes were successfully carried out (Figure S4 and Figure 5). For rGO-SH and GO-SO_3H, S 2p region presented two signals at ca. 164 and 169 eV, which corresponded to H–S–C and S–O, respectively (Figure 5).[74] S 2p signals are characterized by asymmetric peaks due to the spin-orbit splitting of the S 2p level into S $2p_{3/2}$ and S $2p_{1/2}$ (splitting factor 1.1–1.3 eV).[73] Noteworthy, the presence of C–S–H contributions for GO-SO_3H confirmed the incomplete oxidation of the thiol groups. For this catalyst, the XPS S 2p region was deconvoluted into the following contributions: 164.5 eV (H–S–C $2p_{3/2}$), 165.6 eV (H–S–C $2p_{1/2}$), 168.5 eV (S–O $2p_{3/2}$) and 169.8 eV (S–O $2p_{1/2}$). The absence of peaks at around 164.0 eV in rGO-HSO_3Cl and rGO-SO_3H indicated that all the sulfur was in the oxidized form (169.0 eV). The contribution of the different components in each material are summarized in Table S1–Table S6.

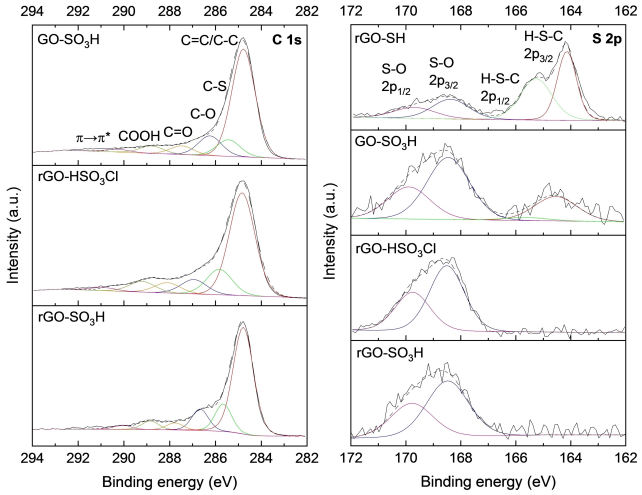

Figure 5. XPS spectra of C 1s for rGO-SO_3H, rGO-HSO_3Cl and GO-SO_3H; S 2p for rGO-SO_3H, rGO-HSO_3Cl, rGO-SH and GO-SO_3H.

The microstructure and morphology of the graphene-based materials were studied by Scanning Electron Microscopy (SEM) and the elemental compositions were determined by Energy Dispersive X-ray spectroscopy (EDS) mapping. SEM images of different samples revealed structures with crumpling agglomerated layers and exfoliated edges.[36,67,75] After sulfonation processes, SEM images revealed unaltered graphene sheets (Figure 6a, Figure 7a and Figure 8a), which could have a positive influence on catalytic activity due to the favored accessibility to the active sites in crumpled morphology layers.[36] Figure 7a revealed that the layer thickness was approximately 0.25 μm which is in concordance with bibliography.[76] The roughness in rGO-SO_3H and GOSO_3H could be ascribed to the thermal impact during the sulfonation process. The elevated reaction temperature may induce the separation of oxygenated functional groups from the structure of GO, resulting in an increased formation of defects.[77] The EDS mapping showed the atomic composition of C, O, Cl and S in sulfonated graphene materials. As shown in Figure 6b, Figure 7b and Figure 8b, S was

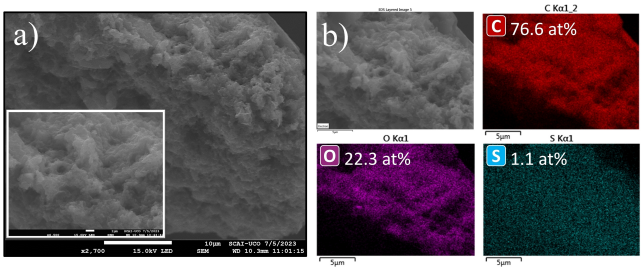

Figure 6. a) SEM image of rGO-SO_3H. b) C, O and S EDS elemental mapping of rGO-SO_3H.

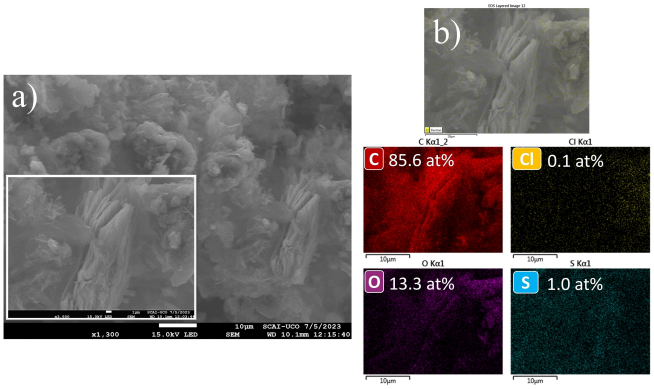

Figure 7. a) SEM image of rGO-HSO_3Cl. b) C, Cl, O and S EDS elemental mapping of rGO-HSO_3Cl.

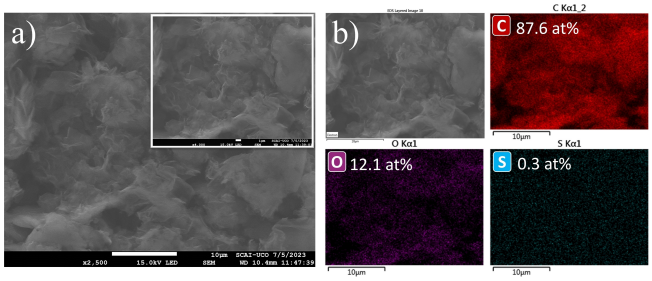

Figure 8. a) SEM image of GO-SO_3H. b) C, O, S EDS elemental mapping of GO-SO_3H.

homogenously dispersed on the surface of the synthesized materials with the following at%: 1.1 %, 1.0 % and 0.3 % for rGO-SO_3H, rGO-HSO_3Cl and GO-SO_3H, respectively. Although these values are in concordance with those obtained by XPS surface analysis, significant differences have been exhibited compared with elemental analysis. However, XPS and EDS quantification are highly dependent of the analyzed area and elemental distribution may not be representative enough.

2.2. Catalytic Tests: Acetalization of Glycerol for Solketal Synthesis

The acetalization reaction of glycerol yields two different products consisting of the 5-(solketal) and 6-membered cycles (Scheme 1), which were the only products detected under the reaction conditions employed.

Table 2 shows the reaction results obtained. As can be seen, the non-functionalized solids, i.e. without sulfonic acid groups in the structure, did not show any catalytic performance, as expected (entries 1–4).

Regarding the catalytic results, almost complete conversion was obtained with the sulfonated graphene-based materials rGO-SO_3H and GO-SO_3H at 50 °C after 60 min of reaction time, whereas a 75 % of conversion was obtained over rGO-HSO_3Cl. This lower value obtained with rGO-HSO_3Cl might be attributed to its lower acidity. In addition, the reaction primarily leads to the formation of solketal, with only small amounts of the six-membered-ring compound, below 5 %, which agrees with results obtained in literature,[78–80] since the 5-membered ring ketal is thermodynamically more stable than the 6-membered ring ketal. Considering the good catalytic results obtained under these conditions, the reaction was carried out at lower temperature, which is more interesting from an economic and environmental point of view. The results of both, glycerol conversion and selectivity to solketal, are shown in Table 2. Even though all sulfonated graphene materials were highly active, more differences among the catalysts can be observed in comparison with the results obtained at 50 °C. The best glycerol conversion value (95 %) was obtained over the rGO-SO_3H catalyst, followed by the GO-SO_3H (70 %) and by rGO-HSO_3Cl (45 %). Considering the acidity exhibited by sulfonated graphene-based materials (mmol SO_3H/g) given in Table 2, it

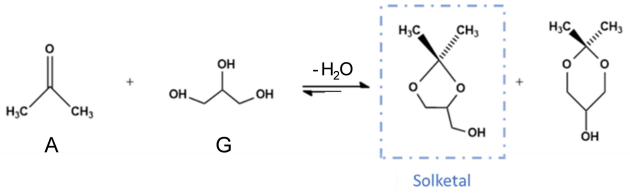

Scheme 1. Acetalization of glycerol (G) with acetone (A).

Table 2. Glycerol conversion, selectivity to solketal and acid properties of the synthesized materials.

Sample	XG (%mol)		Sel (%mol)		Acidity (mmol SO3H/g)c	Density of acid sites (mmol SO3H/m2)×10^{-3}
Graphite	–	–	–	–	–	–
GO	–	–	–	–	–	–
rGO	–	–	–	–	–	–
rGO-SH	–	–	–	–	–	–
GO-SO_3H	95[a]	70[b]	95[a]	95[b]	0.86[c]	6.4
rGO-HSO_3Cl	75[a]	45[b]	97[a]	95[b]	0.34	1.4
rGO-SO_3H	98[a]	95[b]	98[a]	97[b]	0.64	7.5

[a] Reaction conditions: G:A molar ratio 1:12; 5 % w/w catalyst; T = 50 °C; reaction time: 60 min. [b] Room temperature. [c] Acidity was calculated considering the sulfur measured from Elemental Analysis. [d] Calculated as $S_{measured} \times S_{oxidized}(\%)/100$.

was expected that the catalyst with the highest acidity would yield the best results, as reported in literature by several authors.[80–82] Therefore, to better explain these outcomes, another parameter to be considered is the density of sulfonic groups (mmol SO_3H/m^2) that takes into account the textural properties. If we examine the results in relation to the density of acid sites (mmol SO_3H/m^2), a clear correlation with the achieved conversion emerges. Consequently, rGO-HSO_3Cl, characterized by the lowest acidity and the highest surface area, demonstrated the least effective catalytic performance. In addition, the higher acid strength of aryl-SO_3H moieties in rGO-SO_3H in comparison to alkyl-SO_3H present in GO-SO_3H could also contribute to the differences between their catalytic performances, as previously reported in other reactions catalyzed by sulfonic acid solids, such as the etherification of glycerol.[74,83]

Figure 9 shows the evolution of glycerol conversion with reaction time at room temperature. Two different tendencies can be observed. On the one hand, rGO-SO_3H solid reached the maximum conversion values at only 15 min of reaction time. In addition, at 10 min at room temperature, the glycerol conversion value was 78%. On the other hand, the evolution of the glycerol conversion with time over rGO-HSO_3Cl and GO-SO_3H was less prominent. In fact, at 15 min, the conversion values were 22 and 44%, respectively, which supposes 49% and around 60% of the total conversion achieved for rGO-HSO_3Cl and GO-SO_3H, respectively. To give a possible explanation to this fact, we need to consider several factors. Firstly, in the reaction mechanism of the acetalization reaction, the carbonyl group of acetone is activated by the proton of an acid site, and then, this carbonyl group is attacked by a nucleophilic oxygen of a hydroxyl group from glycerol, forming the hemiketal. In a subsequent attack, by another nucleophilic oxygen, the ketal is finally formed. In this regard, since two successive acid-catalyzed reactions are required for the formation of solketal, a higher density of centers would facilitate its formation. Secondly, the reaction mixture acetone/glycerol is biphasic, with the solketal produced during the reaction favoring the homogenization of the solution.

In addition, a high hydrophobicity of the material could be advantageous in several ways. It facilitates the physisorption of acetone molecules on the catalyst, and, moreover, due to a lower amount of polar groups in the material, it would prevent the hydroxyl (OH) groups of glycerol from forming hydrogen bonds with the free hydroxyl groups present on the surface of the graphene-based material, allowing an easier nucleophilic attack. Indeed, rGO-SO_3H material would exhibit the highest hydrophobicity according to its decreased fraction of oxygenated groups, observed both by XPS (Figure S3 and Tables S4–S6) and XRD (loss of the peak at 11.7°), characteristic of a reduced graphene oxide structure (Figure 2). This fact would explain its higher reaction rate compared to GO-SO_3H and rGO-HSO_3Cl. Furthermore, this hydrophobicity would prevent the water molecules formed during the reaction from getting too close to the solketal that has formed. Due to the acid sites present, water could hydrolyze the ketal formed, thus reversing the course of the reaction.

To contextualize the catalytic results obtained, a comparison of the best performing catalyst reported in this work (rGO-SO_3H) has been carried out in relation to the state of the art recently reported by Cheruvathoor Poulose et al.[84] In terms of productivity of solketal (mmol solketal/g h), our catalyst was very competitive among all evaluated catalysts with a productivity value of 800 mmol solketal/g h, only being outperformed by an aminosulfonic acid-derivatized graphene catalyst (G-ASA) with 2168 mmol solketal/g h.[84]

The reusability of the solids was studied by three consecutive acetalization reactions (Figure 10). As can be seen, all solids behaved in a similar way, experiencing a conversion loss around 5–10% after the first use, and then remaining practically constant. It is important to note that selectivity to solketal is not depicted because it showed no changes, remaining above 95% in all cases.

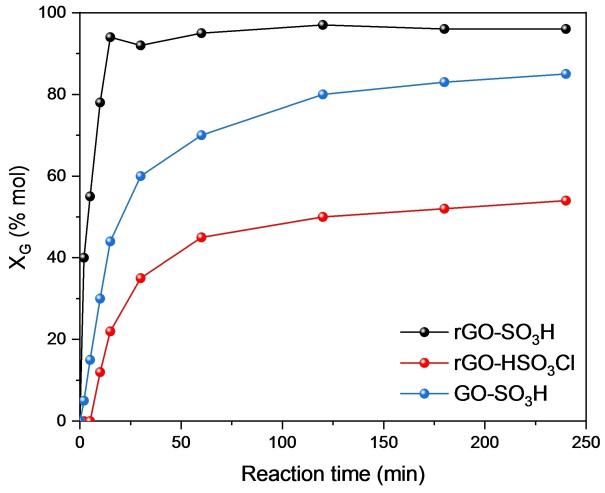

Figure 9. Study of the variation of conversion with time of reaction on the catalysts studied. Reaction conditions: 5.0 wt.% of catalyst referred to the starting amount of glycerol, A/G molar ratio = 12, at room temperature.

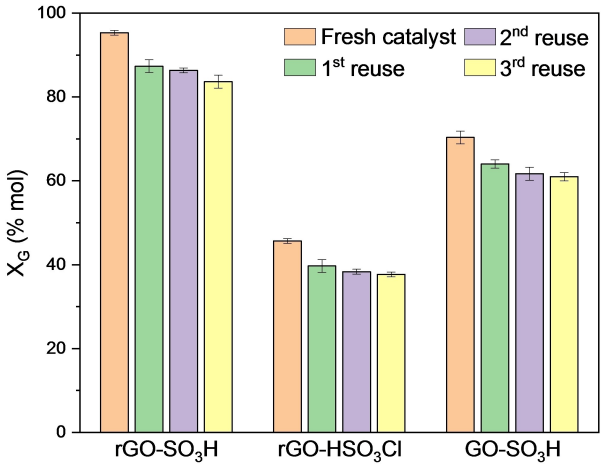

Figure 10. Glycerol conversion on the fresh and reused solids studied under the same experimental conditions as in Figure 9 after 60 min of reaction time.

Despite the excellent activity, selectivity and stability of the catalyst rGO-SO_3H in the reaction studied, its large-scale application could be limited by the environmentally unfriendly synthesis of graphene oxide from graphite by the Hummers method. Clearly, this aspect needs to be resolved and further research in this direction is necessary.

3. Conclusions

Various graphene-based catalysts have been obtained by sulfonation of graphene oxide (GO) following three different strategies. The higher sulfur content and acidity was achieved by thiolation followed by oxidation, resulting in the GO-SO_3H material, which had both sulfonic acid (77%) and thiol groups (23%) and mainly possessed a graphene oxide structure. The direct treatment of GO with chlorosulfonic acid gave the rGO-HSO_3Cl material with a partially reduced structure, which presented the highest specific surface area. In contrast, the rGO-SO_3H material, with a reduced graphene oxide structure, was obtained after hydrothermal treatment followed by sulfonation with fuming sulfuric acid and showed the lowest specific surface area. The latter two contained all the sulfur in oxidized form. Catalyst rGO-SO_3H exhibited the highest activity in the acetalization reaction of glycerol with acetone at room temperature (95% conversion at 15 min) with 98% selectivity towards solketal. All three catalysts showed only a small loss of activity during four consecutive runs, after which the conversion remained above 83% with a selectivity over 95% for rGO-SO_3H. The superior catalytic activity of rGO-SO_3H for the production of solketal by acetalization of glycerol with acetone was apparently due to its higher density of acid sites and hydrophobicity. Ultimately, sulfonated graphene-based materials could be promising catalysts for many other biomass valorization processes that require acid catalysts.

Experimental Section

Reagents and Materials

GO derivatives were synthesized using the following commercial reagents: graphite powder (Aldrich), sodium nitrate (PanReac), sulfuric acid (PanReac, 95–98%), potassium permanganate (Aldrich, 99%), hydrogen peroxide (PanReac, 30%), hydrochloric acid (GlobalChem, 37%), fuming sulfuric acid (Aldrich, 30%), dichloromethane (Labkem, anhydrous, $>$99.8%), chlorosulfonic acid (Aldrich, 99%, ethanol (Sigma Aldrich, 99%), diethyl ether (PanReac, 99.7%), hydrobromic acid (PanReac, 48%), thiourea (Sigma Aldrich, 99%), potassium hydroxide (PanReac, 85%), dimethylformamide (PanReac, 99.8%).

Synthesis of Graphene Oxide (GO)

Graphene oxide (GO) was synthesized by a modified Hummers method[85] using graphite as starting material. Graphite (3 g) and sodium nitrate (1.5 g) were added to concentrated sulfuric acid (70 mL) under stirring. The mixture was cooled to 0 °C and potassium permanganate (9 g) was added slowly to keep temperature at 20 °C. After 15 min, the reaction was kept at 40 °C for 30 min. Then, 140 mL of water was added, and was stirred for 15 min at 90 °C. Hydrogen peroxide was slowly added and the temperature was turned off meanwhile the system was continuously stirred. Then, the product was filtered and washed with hydrochloric acid (10%) and centrifuged with deionized water (3500 rpm for 10 min each time) until pH of supernatant was ca. 7. After that, the material was dried at 60 °C overnight. Finally, a milling ball was used to obtain the powder.

Synthesis of Thermal Reduced Sulfonated Graphene Oxide (rGO-SO_3H)

GO was thermally reduced by hydrothermal treatment. 80 mg of the as-prepared GO was added into 40 mL of deionized water followed by 1 h ultrasonication to fully disperse the material. The resulting solution was transferred to a teflon line autoclave and the synthesis was carried out at 200 °C for 15 h. Then, it was filtered and lyophilized to obtain the material denoted rGO.

rGO (0.5 g) was added into 25 mL of fuming sulfuric acid. The solution was homogenized in an ultrasonic bath for 1 h. The synthesis was carried out in a teflon line autoclave at 180 °C for 24 h. Then, the material was filtered and washed several times with deionized water. Finally, the obtained material, rGO-SO_3H, was dried under vacuum at 80 °C for 12 h.[46]

Synthesis of Partially Reduced Sulfonated Graphene Oxide (rGO-HSO_3Cl)

The synthesis of rGO-HSO_3Cl was achieved adding 0.5 g of GO into 4 mL of dichloromethane and 1.5 mL of chlorosulfonic acid and the mixture was stirred at room temperature for 24 h under nitrogen atmosphere. Subsequently, the material was washed with deionized water and ethanol several times. Finally, the material was filtered and dried under vacuum at 90 °C for 24 h.[56]

Synthesis of Sulfonated Graphene Oxide (GO-SO_3H) Using Thiol Graphene Oxide (rGO-SH)

First, GO was washed twice with diethyl ether, followed by an ultrasonication treatment in 1.5 L of deionized water for 2 h. Then, 75 mL of hydrobromic acid was added dropwise and was kept under stirring for 45 min. Subsequently, thiourea (75 g) was added while stirring and then the reaction mixture was kept at 70 °C for 24 h. After this time, the mixture was cooled, and 750 mL of potassium hydroxide (3 M) was added while stirring for 45 min. After that, the solid was recovered by filtration under vacuum. The resulting material was washed several times with water, dimethylformamide, diethyl ether and ethanol to remove possible reagent residues. Finally, the synthesized material, rGO-SH, was dried under vacuum at room temperature for 3 days.[73]

rGO-SH (0.27 g) was oxidized with 80 mL of hydrogen peroxide (30%) at 90 °C for 24 h. After that, the material was washed with 25 mL of sulfuric acid (1.2 M) prior to filtering and washing with ethanol. Finally, the material was dried under vacuum at 120 °C for 24 h. The obtained material was denoted GO-SO_3H.[56]

Characterization

X-ray powder diffraction (XRD) patterns were collected over the 2θ range 3–80° in a Bruker D8 Discover A25 diffractometer using Cu Kα radiation. Raman spectra were acquired in a Renishaw Raman instrument with green laser light (532 nm) over the wavenumber

range 150–4000 cm^{-1}. Elemental analysis results were obtained by combustion of the material and was performed on a CHSN TM FlashSmart elemental analyzer (Thermo Scientific). Sulfur content was revealed by dynamic combustion (modified DUMAS method 10 min) in an elemental reactor followed by a reduction process, completed by gas chromatographic separation and detection of the products by a thermal conductivity detector (TCD). The OEA/FPD option increases the sensitivity to sulfur (5 ppm) through the use of a Photometric Flame Detector (FPC) coupled to the system. Nitrogen adsorption-desorption isotherms were obtained in a Micromeritics ASAP 2020 system at −196 °C. Samples were outgassed at 120 °C before the measurement. BET was used for determining the specific surface area. XPS measurements were performed using a SPECS mod. PHOIBOS 150 MCD spectrometer using monochromatic Mg Kα radiation and a multichannel detector. The samples were outgassed in an ultra-high vacuum multipurpose surface analysis system Specs. The binding energy (eV) calibration has been referred to carbon 1 s peak (284.8 eV). Scanning electron micrographs was obtained with a JEOL JSM 7800 microscope at a voltage of 15 kV.

The acidity of rGO-HSO_3Cl and rGO-SO_3H was calculated as the amount of sulfur measured by elemental analysis, since all the sulfur in the materials is in sulfonic form. In the GO-SO_3H solid, the acidity was calculated considering both the amount of sulfur measured by elemental analysis and the percentage of oxidized sulfur measured by XPS (Table S6), as follows:

$$\text{mmol } SO_3H = S_{measured} \times S_{oxidized}(\%)/100$$

Catalytic Tests

Acetalization of glycerol (≥99.5%, SigmaAldrich) with acetone (≥99.5%, Sigma–Aldrich) was carried out in a Syrris–Orbit Multireactor. The total volume employed was 5 mL to ensure the optimal sample temperature control. In this sense, the amount of glycerol (limiting reagent) employed was 0.47 g, and the molar ratio acetone/glycerol was 12. These parameters together with the catalyst loading (5% w/w, referred to initial glycerol mass) were selected in accordance with the results obtained in a previous study about the reaction parameters optimization by an ANOVA statistical test.[79] Vessels are made of Pyrex glass with a total volume of 25 mL. After time of reaction, under magnetic stirring at autogenous pressure, the reactor vessel was cooled down in an ice bath and the sample was filtered off and subsequently analyzed. The quantitative analysis was carried out by Gas Chromatography in an Agilent Technologies 7890 A GC System, equipped with a Supelco 25357 NukolTM capillary column and a Flame Ionization Detector (FID), using N,N-dimethylformamide (≥99.9% Sigma–Aldrich) as an internal standard, according with a previous procedure.[80] Glycerol conversion (X_G) and solketal selectivity (Sel) were determined by means of Eqs. 1 and 2:

$$X_G(\%) = \frac{\textbf{mmol of products}}{\textbf{starting mmol of G}} \times 100 \quad (1)$$

$$\text{Sel}(\%) = \frac{\textbf{\textit{mmol of solketal}}}{\textbf{\textit{mmol of products}}} \times 100 \quad (2)$$

Blank experiments did not show glycerol conversion under the studied experimental conditions. Recycling experiments were performed over the catalysts tested. At the end of the reaction, the catalysts were filtered off, washed with ethanol (99.5%, PanReac AppliChem) and dried at 80 °C. Afterwards, they were tested again under the same reaction conditions following the above-mentioned procedure.

Acknowledgements

The authors wish to acknowledge the financial support from Andalusian Regional Government (Project ProyExcel_00492 and FQM-346 group), Feder Funds, Spanish Ministry of Science and Innovation (Mecanismo de Recuperación y Resiliencia de la Unión Europea-Next Generation EU) for the projects PID2019-104953RB-I00/MCIN/AEI/10.13039/501100011033, FEDER,UE, PID2022/42657OB-I00/MCIN/AEI/10.13039/501100011033/FEDER,UE, TED2021-132224B-I00/ NextGenerationEU/PRTR, PID2022-142275OB-I00/MCIN /AEI /10.13039/501100011033/FEDER,UE, and PDC2022-133973-I00/AEI/10.13039/501100011033/FEDER,UE, the technical staff from the Instituto Químico para la Energía y el Medioambiente (IQUEMA) and Servicios Centrales de Apoyo a la Investigación (SCAI) de la Universidad de Córdoba (Spain). J. A.-G. would like to thank the fellowship for University Teacher Training (FPU) with reference FPU17/03981 funded by Ministry of Science, Innovation and Universities (Spanish Government), and "Juan de la Cierva" fellowship with reference JDC 2022–048903-I, funded by MCIN/AEI/10.13039/ 501100011033 and the European Union "NextGenerationEU"/PRTR". R. R.-L appreciates the support of Ministry of Science, Innovation and Universities (Spanish Government, State Research Agency, European Union) for the predoctoral contract for the training of doctors (FPI) with reference PRE2019-089122. A. Benítez is supported by a "Juan de la Cierva – Incorporación" fellowship (IJC2020-045041-I), funded by MCIN/AEI/10.13039/501100011033 and the European Union "NextGenerationEU/PRTR", and by Plan Propio de Investigación 2023 de la Universidad de Córdoba (UCOLIDERA, OLIVE2BATTERY project). Funding for open access charge: Universidad de Córdoba/CBUA.

Conflict of Interests

The authors declare no conflict of interest.

Data Availability Statement

The data that support the findings of this study are available from the corresponding author upon reasonable request.

Keywords: graphene oxide · sulfonated graphene · heterogeneous catalysis · glycerol acetalization · solketal synthesis

[1] J. N. Armor, *Appl. Catal. B* **1992**, *1*, 221–256.
[2] J. N. Armor, *Catal. Today* **2011**, *163*, 3–9.
[3] G. Busca, *Chem. Rev.* **2007**, *107*, 5366–5410.
[4] Á. Molnár, in *Encycl. Catal.*, Wiley, **2011**.
[5] P. Gupta, S. Paul, *Catal. Today* **2014**, *236*, 153–170.

[6] S. Liu, M. Zhu, M. Iqbal, *Catal. Surv. from Asia* **2020**, *24*, 196–206.
[7] A. Corma, *Curr. Opin. Solid State Mater. Sci.* **1997**, *2*, 63–75.
[8] K. Tanabe, *Appl. Catal. A* **1999**, *181*, 399–434.
[9] R. Sheldon, R. Downing, *Appl. Catal. A* **1999**, *189*, 163–183.
[10] K. Shimizu, A. Satsuma, *Energy Environ. Sci.* **2011**, *4*, 3140.
[11] J. Dědeček, E. Tabor, S. Sklenak, *ChemSusChem* **2019**, *12*, 556–576.
[12] A. Bhan, E. Iglesia, *Acc. Chem. Res.* **2008**, *41*, 559–567.
[13] M. Kaur, S. Sharma, P. M. S. Bedi, *Chin. J. Catal.* **2015**, *36*, 520–549.
[14] P. Ferrini, J. Dijkmans, R. De Clercq, S. Van de Vyver, M. Dusselier, P. A. Jacobs, B. F. Sels, *Coord. Chem. Rev.* **2017**, *343*, 220–255.
[15] M. A. Harmer, Q. Sun, *Appl. Catal. A* **2001**, *221*, 45–62.
[16] Y. Chauvin, D. Commereuc, F. Dawans, *Prog. Polym. Sci.* **1977**, *5*, 95–226.
[17] A. Fihri, C. Len, R. S. Varma, A. Solhy, *Coord. Chem. Rev.* **2017**, *347*, 48–76.
[18] X. Song, A. Sayari, *Catal. Rev.* **1996**, *38*, 329–412.
[19] N. Mizuno, M. Misono, *Curr. Opin. Solid State Mater. Sci.* **1997**, *2*, 84–89.
[20] A. P. Wight, M. E. Davis, *Chem. Rev.* **2002**, *102*, 3589–3614.
[21] L. J. Konwar, P. Mäki-Arvela, J.-P. Mikkola, *Chem. Rev.* **2019**, *119*, 11576–11630.
[22] K. S. Novoselov, A. K. Geim, S. V. Morozov, D. Jiang, Y. Zhang, S. V. Dubonos, I. V. Grigorieva, A. A. Firsov, *Science* **2004**, *306*, 666–669.
[23] K. S. Novoselov, V. I. Fal'Ko, L. Colombo, P. R. Gellert, M. G. Schwab, K. Kim, *Nat. 2012 4907419* **2012**, *490*, 192–200.
[24] A. K. Geim, *Science* **2009**, *324*, 1530–1534.
[25] M. S. A. Bhuyan, M. N. Uddin, M. M. Islam, F. A. Bipasha, S. S. Hossain, *Int. Nano Lett. 2016 62* **2016**, *6*, 65–83.
[26] A. Gutiérrez-Cruz, A. R. Ruiz-Hernández, J. F. Vega-Clemente, D. G. Luna-Gazcón, J. Campos-Delgado, *J. Mater. Sci.* **2022**, *57*, 14543–14578.
[27] O. C. Compton, S. T. Nguyen, *Small* **2010**, *6*, 711–723.
[28] A. Razaq, F. Bibi, X. Zheng, R. Papadakis, S. H. M. Jafri, H. Li, *Materials (Basel).* **2022**, *15*, 1012.
[29] R. Tarcan, O. Todor-Boer, I. Petrovai, C. Leordean, S. Astilean, I. Botiz, *J. Mater. Chem. C* **2020**, *8*, 1198–1224.
[30] Y. Zhu, S. Murali, W. Cai, X. Li, J. W. Suk, J. R. Potts, R. S. Ruoff, *Adv. Mater.* **2010**, *22*, 3906–3924.
[31] D. Haag, H. H. Kung, *Top. Catal.* **2014**, *57*, 762–773.
[32] P. Tang, G. Hu, M. Li, D. Ma, *ACS Catal.* **2016**, *6*, 6948–6958.
[33] S. Navalon, A. Dhakshinamoorthy, M. Alvaro, H. Garcia, *Chem. Rev.* **2014**, *114*, 6179–6212.
[34] M. Hara, T. Yoshida, A. Takagaki, T. Takata, J. N. Kondo, S. Hayashi, K. Domen, *Angew. Chem. Int. Ed.* **2004**, *43*, 2955–2958.
[35] K. Nakajima, M. Hara, *ACS Catal.* **2012**, *2*, 1296–1304.
[36] J. Ji, G. Zhang, H. Chen, S. Wang, G. Zhang, F. Zhang, X. Fan, *Chem. Sci.* **2011**, *2*, 484–487.
[37] A. Tawfik, M. Eraky, M. N. Khalil, A. I. Osman, D. W. Rooney, *Environ. Chem. Lett.* **2023**, *21*, 1093–1116.
[38] B. Garg, T. Bisht, Y.-C. Ling, *Molecules* **2014**, *19*, 14582–14614.
[39] N. Yadav, G. Yadav, M. Ahmaruzzaman, *Ind. Crops Prod.* **2024**, *210*, 117999.
[40] I. Zahid, M. Ayoub, B. B. Abdullah, M. H. Nazir, M. Ameen, Zulqarnain, M. H. Mohd Yusoff, A. Inayat, M. Danish, *Ind. Eng. Chem. Res.* **2020**, *59*, 20961–20978.
[41] D. M. F. Santos, M. Gonçalves, C. Nobre, P. Brito, F. M. Perez, M. N. Gatti, G. F. Santori, F. Pompeo, *React. 2023, Vol. 4, Pages 569–634* **2023**, *4*, 569–634.
[42] V. O. Samoilov, A. L. Maximov, T. I. Stolonogova, E. A. Chernysheva, V. M. Kapustin, A. O. Karpunina, *Fuel* **2019**, *249*, 486–495.
[43] S. Y. Giraldo, L. A. Rios, N. Suárez, *Fuel* **2013**, *108*, 709–714.
[44] A. Cornejo, I. Barrio, M. Campoy, J. Lázaro, B. Navarrete, *Renewable Sustainable Energy Rev.* **2017**, *79*, 1400–1413.
[45] P. Ranjan, S. Agrawal, A. Sinha, T. R. Rao, J. Balakrishnan, A. D. Thakur, *Sci. Rep.* **2018**, *8*, 12007.
[46] F. Liu, J. Sun, L. Zhu, X. Meng, C. Qi, F.-S. Xiao, *J. Mater. Chem.* **2012**, *22*, 5495.
[47] A. S. Krishna Kumar, S.-J. Jiang, W.-L. Tseng, *J. Environ. Chem. Eng.* **2016**, *4*, 2052–2065.
[48] N. T. Hanh, D. G. Nghiem, N. T. Tinh, N. M. Dat, L. M. Bao, T. T. Buu, P. P. Bao, D. D. Nhan, T. M. Hoang, N. N. Khoa, P. T. Khang, M. T. Phong, H. H. Nguyen, *Biomass Bioenergy* **2023**, *174*, 106823.
[49] A. Ali, Z. S. Khan, M. Jamil, Y. Khan, N. Ahmad, S. Ahmed, *Curr. Appl. Phys.* **2018**, *18*, 599–610.
[50] J. Amaro-Gahete, V. García-Caballero, A. Benítez, D. G. Gil-Gavilán, R. Rojas-Luna, D. Esquivel, A. J. Fernández-Romero, M. Cano, J. J. Giner-Casares, F. J. Romero-Salguero, *J. Electroanal. Chem.* **2023**, *948*, 117800.
[51] N. Oger, Y. F. Lin, C. Labrugère, E. Le Grognec, F. Rataboul, F.-X. Felpin, *Carbon* **2016**, *96*, 342–350.
[52] V. Belessi, D. Petridis, T. Steriotis, K. Spyrou, G. K. Manolis, V. Psycharis, V. Georgakilas, *SN Appl. Sci.* **2019**, *1*, 77.
[53] C. V. Pham, M. Eck, M. Krueger, *Chem. Eng. J.* **2013**, *231*, 146–154.
[54] C. Miranda, A. Ramírez, A. Sachse, Y. Pouilloux, J. Urresta, L. Pinard, *Appl. Catal. A* **2019**, *580*, 167–177.
[55] E. Vessally, A. Hassanpour, R. Hosseinzadeh-Khanmiri, M. Babazadeh, J. Abolhasani, *Monatshefte für Chemie - Chem. Mon.* **2017**, *148*, 321–326.
[56] H. Naeimi, M. Golestanzadeh, *RSC Adv.* **2014**, *4*, 56475–56488.
[57] M. B. Swami, A. H. Jadhav, S. R. Mathpati, H. G. Ghuge, S. G. Patil, *Res. Chem. Intermed.* **2017**, *43*, 2033–2053.
[58] L. Stobinski, B. Lesiak, A. Malolepszy, M. Mazurkiewicz, B. Mierzwa, J. Zemek, P. Jiricek, I. Bieloshapka, *J. Electron Spectrosc. Relat. Phenom.* **2014**, *195*, 145–154.
[59] M. J. Yoo, H. B. Park, *Carbon* **2019**, *141*, 515–522.
[60] D. Morales-Acosta, J. D. Flores-Oyervides, J. A. Rodríguez-González, N. M. Sánchez-Padilla, R. Benavides, S. Fernández-Tavizón, J. A. Mercado-Silva, *Int. J. Hydrogen Energy* **2019**, *44*, 12356–12364.
[61] H. Hou, X. Hu, X. Liu, W. Hu, R. Meng, L. Li, *Ionics* **2015**, *21*, 1919–1923.
[62] A. Benítez, D. Di Lecce, Á. Caballero, J. Morales, E. Rodríguez-Castellón, J. Hassoun, *J. Power Sources* **2018**, *397*, 102–112.
[63] A. Benítez, D. Di Lecce, G. A. Elia, Á. Caballero, J. Morales, J. Hassoun, *ChemSusChem* **2018**, *11*, 1512–1520.
[64] D. He, Z. Kou, Y. Xiong, K. Cheng, X. Chen, M. Pan, S. Mu, *Carbon* **2014**, *66*, 312–319.
[65] X. Hu, Y. Liu, H. Wang, A. Chen, G. Zeng, S. Liu, Y. Guo, X. Hu, T. Li, Y. Wang, L. Zhou, S. Liu, *Sep. Purif. Technol.* **2013**, *108*, 189–195.
[66] L. D. Ramos Riascos, A. E. Ramírez Sanabria, G. A. Torres Rodríguez, A. Sachse, C. D. Miranda Muñoz, *Top. Catal.* **2022**, *65*, 957–965.
[67] M. Sterlin Leo Hudson, H. Raghubanshi, S. Awasthi, T. Sadhasivam, A. Bhatnager, S. Simizu, S. G. Sankar, O. N. Srivastava, *Int. J. Hydrogen Energy* **2014**, *39*, 8311–8320.
[68] K. S. W. Sing, *Pure Appl. Chem.* **1985**, *57*, 603–619.
[69] P. Van der Voort, K. Leus, E. De Canck, *Introduction to Porous Materials*, Wiley, New York, NY, USA, **2019**.
[70] J. Amaro-Gahete, J. A. Salatti-Dorado, A. Benítez, D. Esquivel, V. García-Caballero, M. López-Haro, J. J. Delgado, M. Cano, J. J. Giner-Casares, F. J. Romero-Salguero, *Sustain. Energy Fuels* **2022**, *6*, 1603–1615.
[71] S. Pei, H.-M. Cheng, *Carbon* **2012**, *50*, 3210–3228.
[72] C. K. Chua, M. Pumera, *ACS Nano* **2015**, *9*, 4193–4199.
[73] A. Munir, T. U. Haq, A. Qurashi, H. U. Rehman, A. Ul-Hamid, I. Hussain, *ACS Appl. Energ. Mater.* **2019**, *2*, 363–371.
[74] R. Estevez, I. Iglesias, D. Luna, F. Bautista, *Molecules* **2017**, *22*, 2206.
[75] S. Neelakandan, N. J. K. P. Kanagaraj, R. M. Sabarathinam, A. Muthumeenal, A. Nagendran, *RSC Adv.* **2016**, *6*, 51599–51608.
[76] D. A. Jasim, H. Boutin, M. Fairclough, C. Ménard-Moyon, C. Prenant, A. Bianco, K. Kostarelos, *Appl. Mater. Today* **2016**, *4*, 24–30.
[77] B. A. Arenas-Blanco, E. M. Pérez-Rodríguez, R. C. Hernández, N. Santos-Santos, E. Mejía-Ospino, *Energy Fuels* **2021**, *35*, 20071–20078.
[78] I. Podolean, J. Zhang, M. Shamzhy, V. I. Pârvulescu, J. Čejka, *Catal. Sci. Technol.* **2020**, *10*, 8254–8264.
[79] J. Hidalgo-Carrillo, R. C. Estévez-Toledano, F. J. López-Tenllado, F. M. Bautista, F. J. Urbano, A. Marinas, *J. Taiwan Inst. Chem. Eng.* **2021**, *125*, 297–303.
[80] L. Aguado-Deblas, R. Estevez, M. Russo, V. La Parola, F. M. Bautista, M. L. Testa, *J. Environ. Chem. Eng.* **2022**, *10*, 108628.
[81] D. Nandan, P. Sreenivasulu, L. N. Sivakumar Konathala, M. Kumar, N. Viswanadham, *Microporous Mesoporous Mater.* **2013**, *179*, 182–190.
[82] P. Manjunathan, S. P. Maradur, A. B. Halgeri, G. V. Shanbhag, *J. Mol. Catal. A* **2015**, *396*, 47–54.
[83] J. A. Melero, G. Vicente, G. Morales, M. Paniagua, J. M. Moreno, R. Roldán, A. Ezquerro, C. Pérez, *Appl. Catal. A* **2008**, *346*, 44–51.
[84] A. Cheruvathoor Poulose, M. Medveď, V. R. Bakuru, A. Sharma, D. Singh, S. B. Kalidindi, H. Bares, M. Otyepka, K. Jayaramulu, A. Bakandritsos, R. Zbořil, *Nat. Commun.* **2023**, *14*, 1373.
[85] Y. Xu, K. Sheng, C. Li, G. Shi, *ACS Nano* **2010**, *4*, 4324–4330.

Manuscript received: February 4, 2024
Revised manuscript received: March 22, 2024
Version of record online: ■■, ■■

RESEARCH ARTICLE

Sulfonated graphene-based materials are used as heterogeneous acid catalysts for solketal synthesis under mild conditions. Acid sites density and hydrophobicity are key parameters to obtain the best catalytic performance of reduced sulfonated graphene oxide (rGO-SO_3H) achieving maximum conversion and selectivity in 15 min.

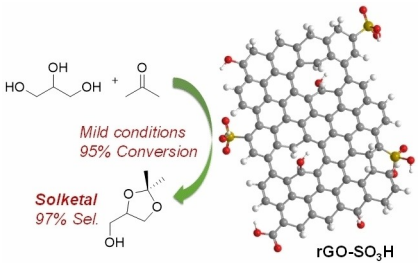

D. G. Gil-Gavilán, Dr. J. Amaro-Gahete, R. Rojas-Luna, Dr. A. Benítez, Prof. R. Estevez*, Prof. D. Esquivel, Prof. F. M. Bautista, Prof. F. J. Romero-Salguero**

1 – 11

Sulfonated Graphene-Based Materials as Heterogeneous Acid Catalysts for Solketal Synthesis by Acetalization of Glycerol